Brazilian Dental Journal (2016) 27(6): 717-726
http://dx.doi.org/10.1590/0103-6440201601028

ISSN 0103-6440

Physico-chemical and Histomorphometric Evaluation of Zinc-containing Hydroxyapatite in Rabbits Calvaria

Alinne Azevedo Pereira da Silva Suruagy[1], Adriana Terezinha Neves Novellino Alves[2], Suelen Cristina Sartoretto[1], José de Albuquerque Calasans-Maia[3], José Mauro Granjeiro[4], Mônica Diuana Calasans-Maia[5]

[1]Post-Graduate Program, Dental School, UFF - Universidade Federal Fluminense, Niterói, RJ, Brazil
[2]Department of Oral Diagnosis, Dental School, UFF - Universidade Federal Fluminense, Niteroi, RJ, Brazil
[3]FFE Department, Dental School, UFF - Universidade Federal Fluminense, Nova Friburgo, RJ, Brazil
[4]Clinical Unit Research, Dental School, UFF - Universidade Federal Fluminense, Niterói, RJ, Brazil
[5]Department of Oral Surgery, Dental School, UFF - Universidade Federal Fluminense, Niterói, RJ, Brazil

Correspondence: Prof. Calasans-Maia, Monica, Rua Mario Santos Braga,28/3º andar, 24020-140 Niterói, RJ, Brazil. Tel:+55-21-2629-9803.

The aim of this study was to characterize the physico-chemical properties and bone repair after implantation of zinc-containing nanostructured porous hydroxyapatite scaffold (nZnHA) in rabbits' calvaria. nZnHA powder containing 2% wt/wt zinc and stoichiometric nanostructured porous hydroxyapatite (nHA - control group) were shaped into disc (8 mm) and calcined at 550 °C. Two surgical defects were created in the calvaria of six rabbits (nZnHA and nHA). After 12 weeks, the animals were euthanized and the grafted area was removed, fixed in 10% formalin with 0.1 M phosphate buffered saline and embedded in paraffin (n=10) for histomorphometric evaluation. In addition, one sample from each group (n=2) was embedded in methylmethacrylate for the SEM and EDS analyses. The thermal treatment transformed the nZnHA disc into a biphasic implant composed of Zn-containing HA and Zn-containing β-tricalcium phosphate (ZnHA/βZnTCP). The XRD patterns for the nHA disc were highly crystalline compared to the ZnHA disc. Histological analysis revealed that both materials were biologically compatible and promoted osteoconduction. X-ray fluorescence and MEV-EDS of nZnHA confirmed zinc in the samples. Histomorphometric evaluation revealed the presence of new bone formation in both frameworks but without statistically significant differences ($p>0.05$), based on the Wilcoxon test. The current study confirmed that both biomaterials improve bone repair, are biocompatible and osteoconductive, and that zinc (2wt%) did not increase the bone repair. Additional *in vivo* studies are required to investigate the effect of doping hydroxyapatite with a higher Zn concentration.

Key Words: zinc, hydroxyapatite, histomorphometric evaluation, calvaria, rabbits

Introduction

The regeneration of bone defects has been extensively studied in oral surgery and dental implantology, and spurred the search for bone substitute materials. Chemical and morphological similarities of calcium phosphates to the inorganic phase of bone make them appropriate for treatment of various bone injuries, like tumors, cysts and other bone diseases (1-3), as well as trauma defects (4). Calcium phosphates (CaPs) have been widely used as biomaterials. In this group of materials, hydroxyapatite [$(Ca_{10}(PO_4)_6(OH)_2)$–(HA)] is most well-known for being crystallographically and chemically similar to the mineralized constituent of hard tissues (5). These characteristics result in excellent cytocompatibility and osteoconductivity. However, it is important to note that native bone apatite differs from stoichiometric HA in several ways i.e., nostoichiometry and nano-sized crystal dimensions (nHA) (6).

In addition, HAs may present a dense or porous form and may or may not be sintered (7-8). The interconnected pores of the HA framework favor cell insertion, adhesion, proliferation and differentiation within their structure and vascularization (7,9), allowing bone to grow and neoformed bone to bond to the HA. However, the sintering process promotes fusion of the HA particles, which decreases their surface area and volume and increases their crystallinity, which results in a less absorbable biomaterial (10).

Zinc, which is a trace element present in bone, is important because it is able to increase mineralization due to its role in the production of extracellular bone matrix (11-13). Bivalent cations, such as Mg^{+2}, Sr^{+2} and Zn^{+2} (13-15) incorporated into the crystalline structure of HA have been studied as a powerful tool for understanding the cellular and molecular mechanisms of the biological mineralization process. Moreover, the HAs modified by Zn incorporation favor the production of cytokines by monocytes, increase chemotaxis and decrease the inflammatory reaction (16). The addition of zinc to the HA structure may improve the osteogenic biologic response of these biomaterials, which is beneficial to graft surgery procedures (11,16-18).

Advances in nanotechnology provide new possibilities for the production of biomimetic surfaces that resemble the *in vivo* cell growth environment on a nanoscale level. Nanotopographical changes in the surfaces of biomaterials can affect positively the bioactivity and osseointegration properties of these biomaterials (19). Nanotechnology

involves the creation of functional materials, devices and systems by controlling matter in the nanometer scale (1–100 nm). The application of nanotechnology to biomedical surfaces is due to the ability of cells to interact with nanometric features (20).

Studies that confirm the positive effects of zinc addition to nanoscale HAs are required. The aim of the current study was to evaluate bone repair after implantation of a porous framework consisting of non-sintered zinc-containing nanostructured hydroxyapatite in rabbit calvaria.

Material and Methods

Biomaterials

The biomaterials were produced at the Brazilian Center for Physical Research (LABIOMAT-CBPF) and characterized before implantation using the X-ray diffraction (XRD), attenuated total reflectance Fourier transform infrared spectroscopy technique (ATR-FTIR) and X-ray fluorescence. Scanning electron microscopy (SEM) was performed at COPPE (UFRJ).

The nanostructured hydroxyapatite (nHA) and nanostructured hydroxyapatite containing 2 wt% zinc (nZnHA) powders were synthesized using calcium nitrate and zinc nitrate solutions (molar zinc contents of 0 and 5 wt%), respectively, and dibasic ammonium phosphate. Calcium nitrate [Ca $(NO_3)_2.4H_2O$] and zinc nitrate [Zn $(NO_3)_2.6H_2O$] solutions with a total cation concentration of 0.2 M were used. Using a peristaltic pump at a flow rate of 4.5 mL/min, this solution was dripped on a dibasic ammonium phosphate solution [i.e., 0.20 M $(NH_4)_2HPO_4$ with a pH of 9.0, which was maintained with concentrated ammonium hydroxide (NH_4OH)] at 37 °C with mechanical agitation (240 rpm).

Next, the mixture underwent digestion for 3 h under the same conditions, and then the mixture was filtered using a Buckner funnel and re-suspended in Milli-Q water at room temperature three times until a pH of 7.0 was obtained in the washing water. The obtained solid was lyophilized (freeze-dried) for 24 h. This procedure was used to prepare all the samples. Finally, the solid was macerated and strained through a <74 µm mesh screen.

The porous nHA and nZnHA discs were prepared using a mixture of 10 g of hydroxyapatite powder (<74 µm) doped with 5% by mass of zinc (ZnHA) or hydroxyapatite without Zn (nHA control) with 9 g of Licowax polyethylene spheres (PE 520; Clariant Produkte, GmbH Gersthofen, Germany). The discs were dried in an oven for 24 h at 50 °C. Next, the discs were placed in aluminum trays followed by heat treatment, which involved calcination for 15 h until 550 °C was achieved. After additional 2 h, a maximum of 700 °C was achieved, resulted in a ramped heat treatment that lasted 17 h. The obtained discs were washed, dried in an oven at 80 °C, sealed in consecutive individual dual plastic packages and sterilized with gamma radiation at UFRJ (15 kg, 10 h), followed by storage at room temperature prior to the surgical procedure.

Biomaterial Characterization Techniques

The biomaterials were characterized before and after implantation to determine their structural and superficial characteristics as well as their chemical compositions.

X-ray fluorescence was performed at the Brazilian Physical Research Center. The nHA and nZnHA macerated discs were employed to record the X-Ray diffractograms, infrared spectra and chemical quantification. The instruments included a powder diffractometer Zeiss HZG4 with CuKa radiation (=1.5418 Å) and angular scanning from 10 – 100º with a passage of 0.05/s and a Fourier transform spectrophotometer (IR-Prestige 21; Schimadzu) equipped with DTGS detector and a KBr beam splitter. Analysis was performed by transmittance with 1% KBr pellets in the infrared region (4000 – 500 cm^{-1}). For X-ray fluorescence, a Phillips model PW-2400/sequential spectrometer was used and the data for Ca, P and Zn were obtained relative to the concentration in % mols/total mol of the samples, melted using a mixture of 0.5 g of the melted calcined sample with 6.0 g of high-purity lithium tetraborate.

After implantation, scanning electron microscopy with secondary electron and energy dispersive spectroscopy (EDS) was performed for bone blocks containing the nHA and nZnHA discs using a Jeol JSM 6490-LV in the Electronic Microscopy Laboratory of the Metallurgical Engineering and Materials Program of the Federal University of Rio de Janeiro (LME-PEMM/COPPE-UFRJ).Animal experiments and breeding were performed under conditions approved by the Institutional Review Board (CEUA/UFF: 163) in compliance with the NIH Guide for Care and Use of Laboratory Animals and the Brazilian legislation on animal use. The animal model was the male white New Zealand rabbit, weighing between 3.000 and 3.500 g at approximately 18 to 20 weeks of age and was obtained from the Veterinary School of Medicine from Universidade Federal Fluminense (UFF). The present study is reported according to the ARRIVE guidelines, in regard of relevant items.

Six animals were randomly selected and euthanized after the experimental period (i.e., 12 weeks) after the surgical procedures for biomaterial implantation had elapsed.

Anesthesia Procedures

The animals were operated under general anesthesia, administered by a veterinary anesthetist using the following anesthetic medication: intramuscular injection of 20 mg/Kg of Ketamine (Francotar®; Virbac do Brasil Comércio e Indústria LTDA, São Paulo, SP, Brasil) and intramuscular injection of 1 mg/Kg of Xylazine (Sedazine®; Fort Dodge

Animal Health, Fort Dodge, IA, USA). Inhalatory anesthetic maintenance was provided by 1% isoflurane (Isoflurane®; Cristália Produtos Químicos e Farmacêuticos Ltda, Itapira, SP, Brazil). Local anesthetic infiltration was performed with 2% lidocaine chloride with epinephrine 1:100,000 (Alphacaine®; DFL Indústria e Comércio SA, Rio de Janeiro, RJ, Brazil) to reduce local bleeding during the surgical procedure. A veterinary anesthesiologist (doctor) monitored the O_2 saturation, arterial pressure and cardiac frequency of the animals during the entire surgical procedure.

Surgical Procedures

First, trichotomy of the calvaria of the animals was performed, and the animals were placed on the operating table lying in ventral decubitus followed by topical degerming using 2% chlorhexidine. Then, sterile surgical clamps were placed to isolate the operating region.

A median sagittal incision approximately 7 cm long was made on the calvarium of the animal using a No. 3 scalpel handle (Bard Parker, Aspen Surgical™ Products, Miami, FL, USA) fitted with a No. 15 C blade (Maxicor Produtos Médicos LTDA, Pinhais, PR, Brazil).

After incision, displacement and exposure of the calvarial bones, two trephinations were made with an 8 mm internal diameter trephine bur (Sistema de Implantes Nacional, São Paulo, SP, Brazil) to a depth of approximately 2 mm at low speed (900 rpm) with intermittent irrigation using a 0.9% sodium chloride solution (Laboratório Sanobiol LTDA, Pouso Alegre, MG, Brazil) to keep the region cool and to prevent tissue necrosis at the site due to overheating.

The nHA and nZnHA implants were adapted to the receptor beds (Fig. 1). The nHA disc (control biomaterial) was placed in the perforation on the right, and the nZnHA disc (test biomaterial) was placed in the perforation on the left. After insertion of the implants, the periosteum was fixed with simple interrupted stitches, and the skin was sutured with simple continuous stitches using monofilament nylon 5.0 thread (ETHICON® :Johnson & Johnson do Brasil Indústria e Comércio de Produtos para a Saúde Ltda, São Paulo, SP, Brazil). The sutured surgical wounds were cleaned with 10 volumes of hydrogen peroxide (Riohex® Indústria Farmacêutica Bioquimica LTDA, São Paulo, SP, Brazil) and a degerming chlorhexidine (Riohex®) solution and left uncovered. To recover from anesthesia, the rabbits were returned to their cages covered by the operative fields to prevent loss of body heat. The animals had access to rations and water *ad libitum* as well as analgesic assistance during the post-operative period, provided by the veterinarians from the School of Veterinary Medicine of UFF.

Histologic Processing

At the end of the 12 week experimental period, the animals received the same anesthetic protocol as previously described for the surgical procedures and were euthanized by cardiac injection of 150 mg of thiopental (Thiopenthax® Cristália Produtos Químicos e Farmacêuticos Ltda, Itapira, SP, Brazil) to collect tissues for histologic processing. The calvaria region that contained the nHA and nZnHA implants in the six animals was removed with a 5 mm safety margin. From five animals, 10 samples were fixed in 10% formaldehyde in a phosphate buffer at a 7.4 pH for 48 h. Then, the tissues were washed in running water for 2 h and placed in a bone decalcifying solution (Allkimia®, Campinas, SP, Brazil) until complete demineralization, for embedment in paraffin. Alternate cuts 5 µm thick and longitudinal to the plane of the implant were performed using a Jung-Leica RM 2045 microtome (Leica Biosystems Inc., Buffalo Grove, IL, USA) followed by staining with the Hematoxylin-Eosin and Masson's trichrome techniques. On the obtained cuts, descriptive histological, histomorphometrical and statistical analyses were performed.

The 2 nHA and nZnHA samples from a single animal were not demineralized but processed for inclusion in resin for characterization by scanning electron microscopy (SEM) and energy dispersive spectroscopy (EDS). These samples were sputter coated with gold prior to analysis. Then, the resin blocks containing the samples were adapted to the microtome (Labcut 1010, EXTEC Corp., Enfield, CT, USA) to obtain 100 µm thick cuts using a diamond disc under constant irrigation with water. The cuts were performed in the central region of the bone defect. Next, the cuts were fixed on glass slides using an ethyl cyanoacrylate-based adhesive (Super Bonder®; Rio de Janeiro, RJ, Brazil), sanded and polished with silicon carbide abrasive papers # 800, #1000, #1200 and #2000 and abundant water until an approximate thickness of 30 to 50 µm was obtained.

Figure 1. Surgical procedure for biomaterial implantation. Two surgical defects were created using an 8-mm trephine bur, and the nHA and nZnHA implants were adapted to the right and left receptor beds, respectively.

The slides were closed with Entellan® (Merck©, Darmstadt, Germany) and a small glass slide, and after 24 h, the slides were observed with a light microscope under polarized light with a compensator.

Histomorphometry and Statistics

Each slide containing a histologic cut from each animal of the area containing the implants, stained with HE, was histomorphometrically analyzed under a light microscope with a clear field (Feldmann Wild Leitz- FWL 1000, BM2000, São Paulo, SP, Brazil). The images were captured using a high-resolution digital camera (SONY®; 5.0 megapixels), with a 20× magnification. The entire area of the bone defect in each slide, which corresponds to one biomaterial per animal, was captured in images that corresponded to 18 fields covered per scan. Therefore, images of the 10 cuts (5 animals) were collected, resulting in 180 digital images without superposition.

The digital images were used for quantification by scoring the structures of interest: neoformed bone and the residual biomaterial. The bone volume density (BV/TV%) was calculated by bone volume over total volume, indicating the fraction of volume of interest that was occupied by bone. For biomaterial volume density (BiomatV/TV%), the same calculation method was applied using the ImagePro-Plus® v. 6.0 program (Media Cybernetics, Silver Spring, Rockville, MD, USA). The areas were expressed in percentage.

The quantification was performed by applying a mesh of 100 points over the 180 photomicrographs. The results of the structures of interest were expressed in percentage points and automatically transferred to a Microsoft Excel® spreadsheet.

The GraphPad Prism (version 5.0) software was used to perform statistical analysis. The quantitative percentage description of the pre-existent bone, neoformed bone, conjunctive tissue and biomaterial was represented by means, standard deviations, medians, coefficients of variation and the Kolgomorov Smirnov tests for distribution of normality and distances. The variability was evaluated at a 5% level of significance. Statistical analysis of the experimental and control groups were performed by parametric comparison between the percentage quantity of BV/TV% and BiomatV/TV% throughout the bone defect area. If the data obtained in the analysis exhibited substantial standard deviations and high coefficients of variation, they would be statistically analyzed using the medians (Wilcoxon paired nonparametric test) at a α=0.05 level of significance.

Results

Characterization of the Biomaterials

X-ray diffractograms of the hydroxyapatite and hydroxyapatite containing 2 wt% zinc were recorded using the macerated samples. The results in Figure 2A and 2B indicate that nZnHA exhibited additional peaks compared to those of nHA, related to the presence of the crystalline phase of the zinc-doped tricalcium phosphate (CaZnTCP).

Figures 3A and 3B show the infrared spectra of the nHa and nZnHA macerated samples, respectively, before implantation, and the spectra contain bands corresponding to the $(PO_4)^{-3}$ functional group in a wavelength range of 1089.781 cm^{-1} to 960.55 cm^{-1}. The peaks at 3574.096 cm^{-1} (nHA) and 3570.238 cm^{-1} (nZnHA) corresponded to the hydroxyl bands (OH^{-1}). There were bands indicative of carbonates for both samples.

X-ray fluorescence of the nZnHA macerated samples revealed that the real zinc content observed in this experimental sample was 2 wt%, representing an incorporation yield of 40% in relation to the theoretical initially proposed value (5% zinc). The Ca/P ratio was 1.67±0.03 for the nHA sample and 1.63±0.03 for the nZnHA sample.

Prior to implantation, SEM images of the nHA and nZnHA discs were obtained by secondary electron emission with gold metallization of the discs. Based on the images obtained at 50x magnification, pores were observed in both discs. However, the pores in the nHA disc were evident compared to those in the nZnHA discs (Figs. 4A and 4B, respectively). In addition, the surface of nZnHA was more compact and uniform. At a 15,000× magnification, the pores of the discs of approximately 100 nm could be visualized in detail (Figs. 4C and 4D).

After implantation, the samples of both groups included in the resin were analyzed by SEM and EDS to determine the elemental composition. In this analysis, at a 1000x magnification (central region of the blocks), the image displayed surfaces with similar heterogeneity as well as areas with fissures (Figs. 5A and 5B). However, at 5000X magnification, the interior of the nHA sample, which has an organized internal tubular system connected to the pores of the disc, was more easily observed by its fissure than the nZnHA sample (Figs. 5C and 5D).

In the elemental chemical composition analysis using EDS, in center of the post-implantation sample, zinc was detected based on a peak with reference to trace amounts of Zn with approximately 300 counts and a Zn percentage weight of 0.16 wt% at 500× magnification (Fig. 6). More calcium was observed in the center of the nZnHA and nHA discs than in the areas at the bone interfaces.

Histologic Analysis

Using light microscopy, the descriptive analysis of the demineralized cuts stained with HE and Masson's trichrome revealed the following:

Group nHA: In this group, There was mature bone at

the periphery of the disc, an area corresponding to the biomaterial and neoformed bone with a spherical aspect and tendency to confluence that formed trabeculae in the region of the interface to the central portion of the defect (Fig. 7A). Mineralized bone tissue was stained red and young bone tissue was stained blue (staining with Masson's Trichrome). There were also areas with conjunctive tissue, blood vessels and medullary fat.

Group nZnHA: In this group, there was neoformed bone with a spherical aspect around the medullar fat with a tendency to confluence and form trabeculae in the region of the interface to the central portion of the defect and spaces corresponding to the biomaterial with greater protein adsorption than in the previous group (Fig. 7B). Bone neoformation with a spherical aspect was observed in this group in the central portion of the defect, and mature bone tissue was observed at its periphery. In some cuts, there were areas with conjunctive tissue and blood vessels.

Statistical Analysis

The means, standard deviations,, Kolmogorov Smirnov normality and distance tests and coefficients of variation for the percentage of bone volume density (BV/TV%) and biomaterial volume density (BiomatV/TV%) throughout the entire area of the bone defect of each experimental group are in Figure 8.

As shown in Figure 8, in comparison to Group nHA, Group nZnHA exhibited a larger volume of neoformed bone and a larger volume of biomaterial. The data obtained in the parametric analysis exhibited large standard deviations and high variation coefficients. Therefore, using the medians, the Wilcoxon paired nonparametric test at level of significance of α=0.05 indicated that these percentages did not present statistically significant differences.

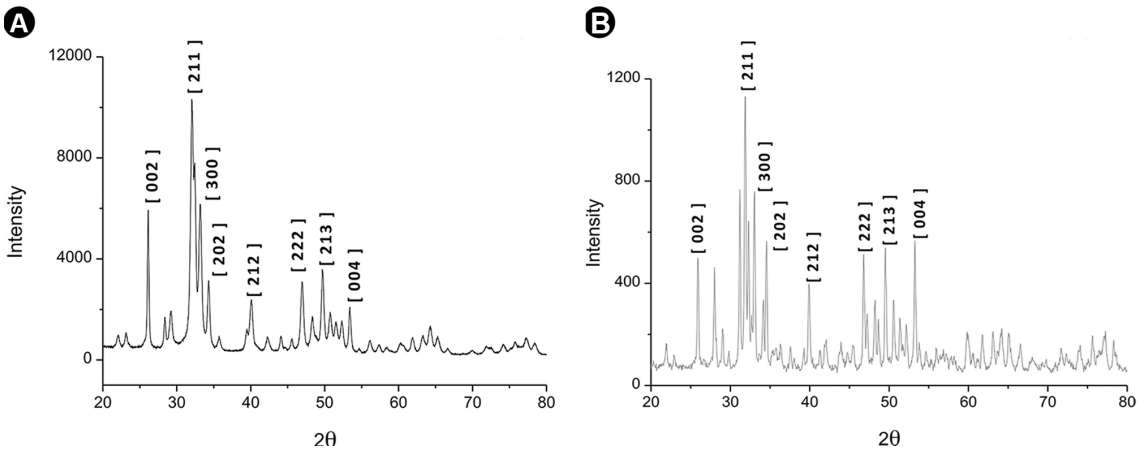

Figure 2. X-ray diffractograms of nHA (A) and nZnHA (B). Observe the additional peaks in the nZnHA x-ray diffractogram, related to the presence of the crystalline phase of zinc -doped tricalcium phosphate.

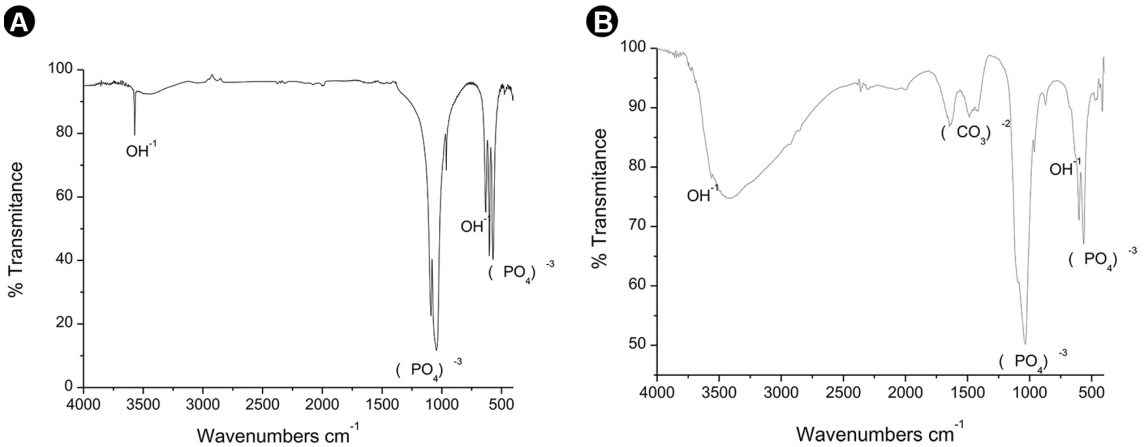

Figure 3. Infrared spectra of the nHa (A) and nZnHA(B). The spectra contain bands corresponding to the (PO4)-3 functional group in a wavelength range of 1089.781 cm-1 to 960.55 cm-1. The peaks at 3574.096 cm-1 (nHA) and 3570.238 cm-1 (nZnHA) correspond to the hydroxyl bands (OH-1). In addition, there are bands indicating presence of carbonates for both samples.

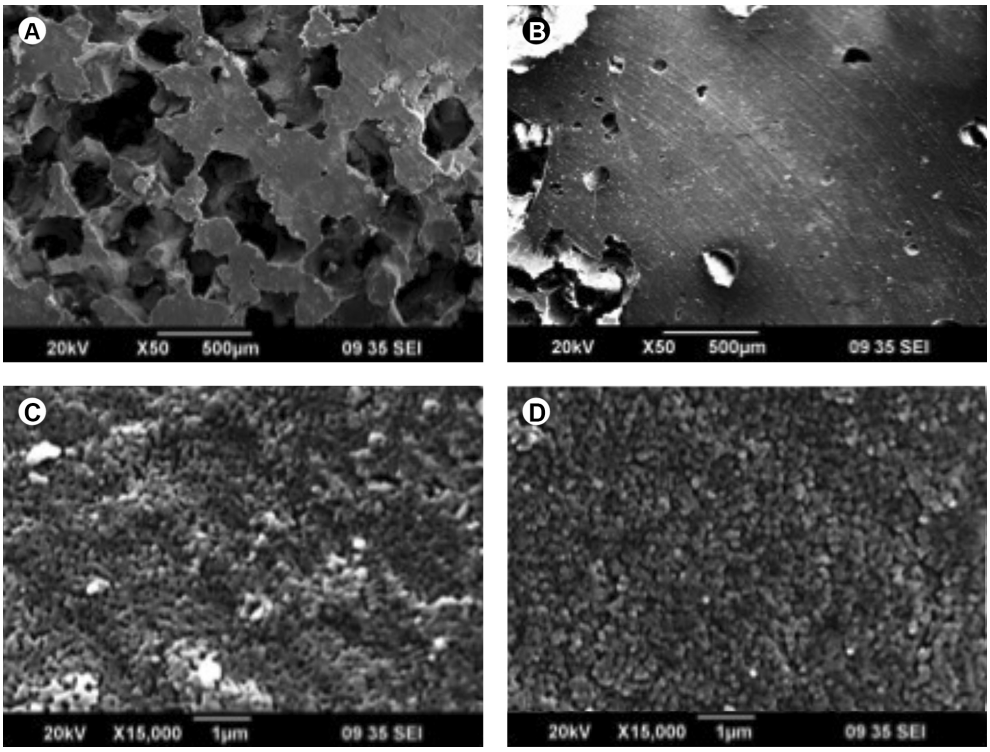

Figure 4. Scanning electron microscopy (SEM) prior to implantation of nHA (A and C) and nZnHA discs (B and D). In the images obtained at 50x magnification (A and B – nHA and nZnHA respectively), observe the presence of pores in both discs, but the pores in the nHA disc were visible compared to those in the nZnHA discs. At a 15000x magnification (C and D – nHA and nZnHA respectively), the surface of nZnHA was more compact and uniform and the pores of the discs of approximately 100 nm may be visualized in detail.

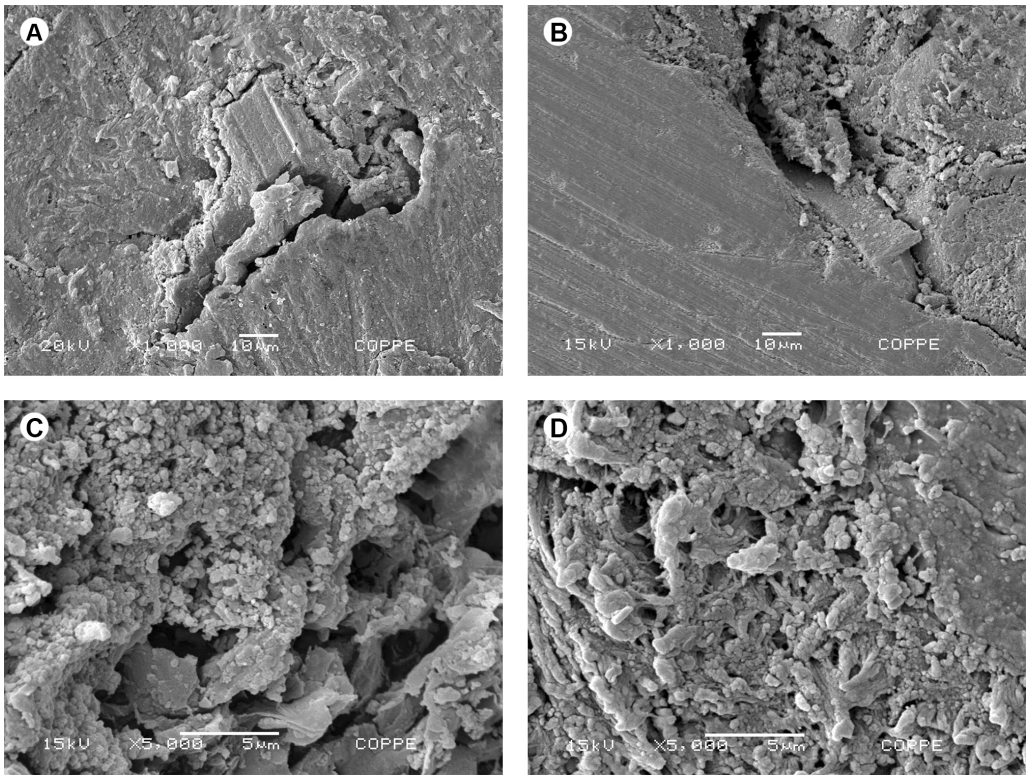

Figure 5. Scanning electron microscopy (SEM) after implantation of nHA (A and C) and nZnHA discs (B and D). In the images obtained at 1000x magnification (A and B – nHA and nZnHA respectively), observe the biomaterial surfaces with similar heterogeneity as well as areas with fissures. At a 5000x magnification (C and D – nHA and nZnHA respectively), the nHA sample, with an organized internal tubular system connected to the pores of the disc, was more easily observed by its fissure than the nZnHA sample.

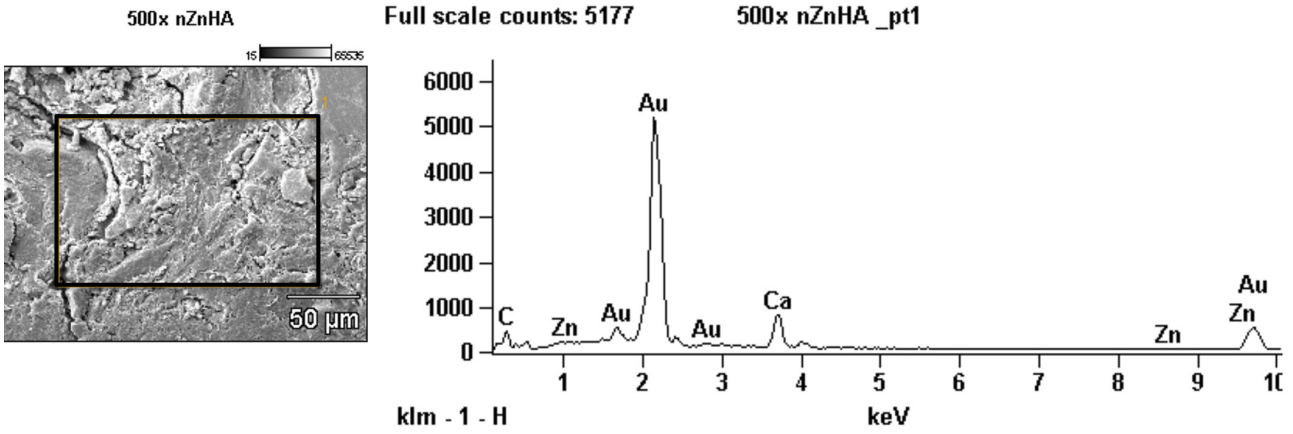

Figure 6. Elemental chemical composition analysis using EDS. The zinc was detected based on a peak with reference to trace amounts of Zn with approximately 300 counts and a Zn percentage of 0.16 wt% at 500x magnification.

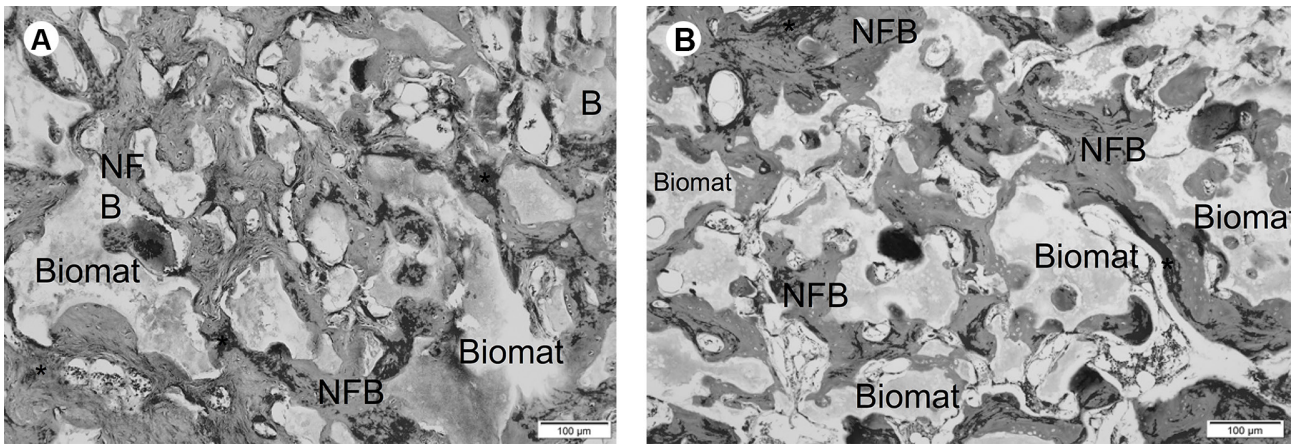

Figure 7. Representative photomicrographs of calvaria defects after 12 weeks. A and B: nHA and nZnHA groups respectively. Biomaterial (B), Neoformed bone (NFB). Masson trichrome stained.

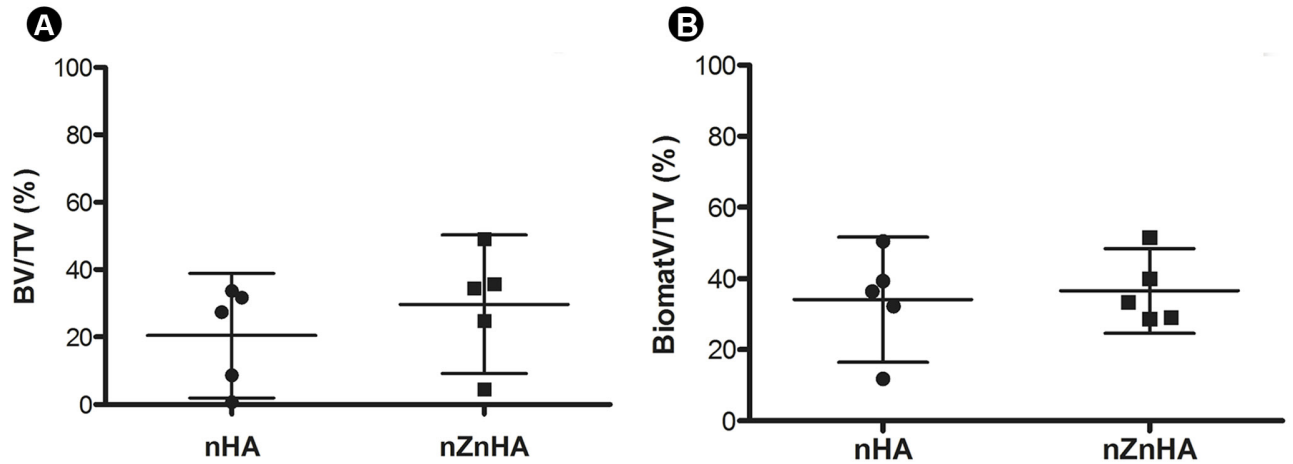

Figure 8. Bone volume density (BV/TV%) (A) and biomaterials volume density (BiomatV/TV%) 4 weeks after implantation. There were no statistical differences between nHA and nZnHA groups. (Wilcoxon paired nonparametric test, $p>0.05$) Results are shown as mean percentages ± confidence interval.

Discussion

The current study used rabbit calvaria as an experimental animal model, which allows for a low cost and easily controlled approach for maintenance and handling after previous training. There are previousstudies (21-23), reporting the advantages of using this experimental model to evaluate the biocompatibility and osteoconduction of a variety of ceramics for bone repair. Among other advantages, the calvaria does not need to be immobilized to prevent fractures, which may occur using mouse, rat and rabbit tibias and femurs (12,24-28). However, due to the thickness of the parietal region of rabbit calvaria, approximately 2 mm, the cutting must be performed carefully.

Despite the use of a medium-sized animal, another reason for selecting the rabbit as an experimental model was that it allowed for a sample with a sufficient number of animals for statistical analysis. Previous reports have confirmed the similarity between the composition, bone mineral density and fracture strength of human and rabbit bones (29).

The experimental period lasted 12 weeks, which is a sufficient time for observing a more advanced stage of bone remodeling in the calvaria of animals because the bone remodeling process lasts approximately six weeks in rabbits. Previous studies used a 5 mm bone defect and an experimental period of 28 days (21) and a critical size defect (15 mm) with an experimental period of 10 weeks (30).

The important characteristics observed for the studied biomaterials include their biocompatibility (31) and osteoconductive properties (26), which serve as a framework for the adsorption of proteins and growth factors that favor the cellular events characteristic of new bone formation, indicating their potential for clinical application as a bone substitute. HA can be prepared in various forms, like blocks, cement, particles (7,26), microspheres (32), cylinders (12,28) and discs (or pellets). The disc form is widely used in neurosurgery for the occlusion of cranial trephination (33). The beneficial effect of the addition of zinc to a nanometric hydroxyapatite-based cement associated with chitosan was also reported, and this material was capable of promoting more new-formed bone, diminishing the gap between the implant and pre-existent bone. This result confirmed the positive effects of zinc on the occlusion of bone defects, like those in the cranium (26).

The incorporation of zinc, an essential trace element for the stimulation of osteoblastic proliferation and inhibition of osteoclastic bone resorption (17,26,34), may improve bone repair, making it an efficient biomaterial for clinical application and justifies its use in this study.

Although previous studies have investigated HA with zinc, this study focused on a nanostructured HA and its effects on *in vivo* bone repair at a 2 wt% zinc concentration, that was not previously studied. Due to the role of zinc in the synthesis of DNA and RNA to stimulate the proliferation of osteoblasts, chondrocytes and fibroblasts, nHa was doped with zinc to optimize or stimulate osteogenesis and/or osteoinduction (35). However, the histomorphometric data, statistically analyzed using the Wilcoxon paired nonparametric test ($p<0.05$), indicated that the 2 wt% zinc did not produce statistically significant differences. Previous histologic and histomorphometric studies of rat calvaria and rabbit tibias (12,25) using ZnHA with 0.5 wt% zinc and ZnHA with 5 wt% zinc, respectively, demonstrated that the response of ZnHA was similar to that of autogenous bone grafts six months after implantation, relative to bone repair. In addition, ZnHA containing 0.5 wt% and 5 wt% zinc were also considered osteoconductors (12,25). However, in comparison to HA, ZnHA did not exhibit statistically significant differences (25).

The results from the X-Ray diffraction identified the nHA sample as a single crystalline phase. The stoichiometric variations and cationic substitutions of HA allowed for zinc doping , resulting in a second phase. FRX chemical analysis indicated a Ca/P ratio of 1.67 ± 0.03 for the HA sample and 1.63 ± 0.03 for the ZnHA sample, confirming stoichiometry of HA. Similar to other studies, the stoichiometric HA was used as control (12,17,36,37) and the presence of another phase (CaZnTCP) was observed in the nZnHA samples.

X-ray diffraction analysis prior to implantation confirmed the synthesis of an nHA with spectra that were very close to those pre-determined by the International Centre For Diffraction Data, which allowed for the fabrication of biomaterials in disc form from nHA and nZnHA spheres of with a degree of purity within the minimum international standards required for biomedical applications.

Comparing the FTIR analyses of the nHA and nZnHA samples, small changes were observed in the phosphate and hydroxyl bands of the nZnHA group compared to those in the nHA Group, due to the migration of OH^- and PO_4^{-3} ions, which are responsible for growth of the new crystalline phase (CaZnTCP). Moreover, the two materials exhibited many similarities in the location of the strong phosphate bands.

The SEM analyses confirmed the porosity of the discs (75%), which provided an excellent pattern for bone neoformation with a spherical aspect in its network of interconnected pores (macroporosity) and cellular adhesion of osteoblasts and fibroblasts to the nHA and nZnHA. These pores were responsible for the 100 ηm microporosity of the disc. In addition, the EDS analyses after implantation indicated trace amounts of zinc (i.e., 0.16 wt%). Based on X-ray fluorescence of nZnHA prior to implantation,

approximately 2 wt% zinc was observed in the whole sample. Therefore, decrease in the percentage of zinc after implantation is due to the greater solubility of the nZnHA samples. The EDS analysis indicated calcium in the discs as well as in the neoformed bone, which confirmed the formation of mineralized bone with osteoid areas, suggesting progressive mineralization of the new bone in the pores and interface region. Previous studies have indicated the importance of macro- and microporosity of graft biomaterials for a large variety of biomedical applications, which supports the histologic and physico-chemical results of the current study (9,10,26,33,38,39).

In conclusion, nanostructured porous hydroxyapatite discs containing 2 wt% zinc were biocompatible and osteoconductive. Both biomaterials favored bone repair. Nevertheless, doping with 2 wt% zinc did not increase bone repair with statistically significant differences compared to that of the control group without zinc.

Resumo

O objetivo deste estudo foi caracterizar físico-químicamente e avaliar o reparo ósseo de discos de hidroxiapatita porosa contendo zinco após a implantação em calvária de coelhos (nZnHA). O pó de nZnHA e o pó hidroxiapatita porosa estequiométrica nanoestruturada (controle – nHA) foram confeccionados em discos (8 mm) e calcinados a 550˚C. Dois defeitos cirúrgicos foram criados na calvária de seis coelhos para a implantação dos discos. Após 12 semanas, os animais foram eutanasiados e as áreas enxertadas foram removidas, fixadas em formol a 10% e embebidas em parafina (n=10) para avaliação histomorfométrica. Além disso, uma amostra de cada grupo (n=2) foi embebida em metilmetacrilato para análise de MEV e EDS. O tratamento térmico dos discos de nZnHA transformou-os em implantes bifásicos compostos por HA contendo Zinco e β fosfato tricálcico com Zinco (ZnHA/βZnTCP). Os discos de nHA, apresentaram-se altamente cristalinos e com baixa solubilidade quando comparados aos discos de ZnHA. A análise histológica revelou que ambos os materiais foram biologicamente compatíveis e promoveram a osteocondução. As análises de FRX e MEV-EDS confirmaram a presença do zinco nas amostras de nZnHA. A avaliação histomorfométrica revelou a presença de neoformação óssea em ambos os grupos, porém sem diferenças estatísticas entre eles, com base no teste de Wilcoxon (p>0,05). O presente estudo confirmou que ambos os biomateriais otimizaram o reparo ósseo, foram biocompatíveis e osseocondutivos e a presença do zinco não favoreceu o reparo ósseo. Estudos adicionais *in vivo* devem ser conduzidos a fim de investigar o efeito de maiores concentrações de zinco.

Acknowledgement

The authors acknowledge the financial support by the Brazilian agencies FAPERJ – Rio de Janeiro Research Foundation and COPPE.

References

1. Tamai N, Myoui A, Kudawara I, Ueda T, Yoshikawa H. Novel fully interconnected porous hydroxyapatite ceramic in surgical treatment of benign bone tumor. Journal of Orthopaedic Science 2010;15:560-568.
2. Calasans-Maia JA, Neto AS, Batista MMD, Alves ATNN, Granjeiro JM, Calasans-Maia MD. Management of ankylosed young permanent incisors after trauma and prior to implant rehabilitation. Oral Surgery 2013: 6:1-7.
3. Al-Sanabani J, Madfa A, Fadhel A. Application of calcium phosphate materials in dentistry. International Journal of Biomaterials 2013;2013:876132.
4. Calasans-Maia MD, Melo BR, Resende RFB, Louro RS, Sartoretto SC, Granjeiro JM, et al.. Cytocompatibility and biocompatibility of nanostructured carbonated hydroxyapatite spheres for bone repair. J Appl Oral Sci 2015;23:599-608.
5. Logeart-Avramoglou D, Anagnostou F, Bizios R, Petite H. Engineering bone: challenges and obstacles. J Cell Mol Med 2005;9:72-84.
6. Rosa AL, Shareef MY, Van Noort R. Efeito das condições de preparação e sinterização sobre a porosidade da hidroxiapatita. Pesqui Odontol Bras 2000;14:273-277.
7. Calasans-Maia MD, Fernandes GVO, Rossi AM, Dias EP, Almeida GDS, Mitri FF, et al.. Effect of hydroxyapatite and zinc-containing hydroxyapatite on osseous repair of critical size defect in the rat calvaria. Key Engeneering Materials 2008;361:1273-1276.
8. Resende RFB, Fernandes GVO, Santos SRA, Rossi AM, Granjeiro JM, Calasans-Maia MD. Long-term biocompatibility evaluation of 0.5% zinc containing hydroxyapatite in rabbits. J Mater Sci Mater Med. 2013;24:1455-1463.
9. Valiense H, Barreto M, Resende RFB, Alves ATNN, Rossi AM, Mavropoulos E, et al.. *In vitro* and *in vivo* evaluation of strontium-containing nanostructured carbonated hydroxyapatite/sodium alginate for sinus lift in rabbits. Journal of Biomedical Materials Research. Part B, Applied Biomaterials 2015;104:274-282.
10. Costa NMF, Yassuda DH, Sader MS, Fernandes GVO, Soares GA, Granjeiro JM. Osteogenic effect of tricalcium phosphate substituted by magnesium associated with Genderm® membrane in rat calvarial defect model. Materials Science & Engineering C, Biomimetic Materials, Sensors and Systems 2016;61:63-71.
11. Grandjean-Laquerriere A, Laquerriere P, Jallot E, Nedelec JM, Guenounou M, Laurent-Maquin D, et al.. Influence of the zinc concentration of sol-gel derivated zinc substituted hydroxyapatite on cytokine production by human monocytes *in vitro*. Biomaterials 2006;27:3195-3200.
12. Wang G, Moya S, Lu Z, Gregurec D, Zreiqat H. Enhancing orthopedic implant bioactivity: refining the nanotopography. Nanomedicine 2015;10:1327-1341.
13. Bressan E, Sbricoli L, Guazzo R, Tocco I, Roman M, Vindigni V, et al.. Nanostructured surfaces of dental implants. Int J Mol Sci 2013;14:1918-1931.
14. Barbosa DZ, de Assis WF, Shirato FB, Moura CC, Silva CJ, Dechichi P. Autogenous bone graft with or without perforation of the receptor bed: histologic study in rabbit calvaria. Int J Oral Maxillofac Implants 2009;24:463-468.
15. Kim HW, Shin SY, Kim HE, Lee YM, Chung CP, Lee HH, et al.. Bone formation on the apatite-coated zirconia porous scaffolds within a rabbit calvarial defect. J Biomater Appl 2008;22:485-504.
16. Yamaguchi M, Yamaguchi R. Action of zinc on bone metabolism in rats. Increases in alkaline phosphatase activity and DNA content. Biochem Pharmacol 1986;35:773-777.
17. Fernandes GVO, Calasans-Maia MD, Mitri FF, Bernardo VG, Rossi AM, Almeida GDS, et al.. Histomorphometric analysis of bone repair in critical size defect in rats calvaria treated with hydroxyapatite and zinc-containing hydroxyapatite 5%. Key Eng Mater 2009;396:15-18.
18. Fernandes GVO, Cortês JA, Melo BR, Rossi AM, Granjeiro JM, Calasans-Maia, MD, et al.. Cytocompatibility and structural arrangement of the collagen fibers: an *in vitro* and *in vivo* evaluation of 5% zinc containing hydroxyapatite granules. Key Eng Mater 2012;493:298-303.
19. Kawamura H, Ito A, Muramatsu T, Miyakawa S, Ochiai N, Tateishi T. Long-term implantation of zinc-releasing calcium phosphate ceramics in rabbit femora. J Biomed Mater Res A 2003;65:468-474.
20. Wang X, Mabrey JD, Agrawal CM. An interspecies comparison of bone fracture properties. Biomed Mater Eng 1998;8:1-9.
21. David LR, Gewalli F, Guimãraes-Ferreira J, Sanger C, Glazier S, Argenta LC. Dynamic spring-mediated cranioplasty in a rabbit model. J Craniofac Surg 2002;13:794-801.
22. Habibovic P, Kruyt MC, Juhl MV, Clyens S, Martinetti R, Dolcini L, et al.. Comparative *in vivo* study of six hydroxyapatite-based bone graft substitutes. J Orthop Res 2008;26:1363-1370.
23. Ito A, Senda K, Sogo Y, Oyane A, Yamazaki A, Legeros RZ. Dissolution

rate of zinc-containing β-tricalcium phosphate ceramics. Biomed Mater 2006;1:134-139.
24. Ripamonti U, Richter PW, Nilen RW, Renton L. The induction of bone formation by smart biphasic hydroxyapatite tricalcium phosphate biomimetic matrices in the non-human primate *Papio ursinus*. J Cell Mol Med 2008,12:2609-2621.
25. Santos MH, Valerio P, Goes AM, Leite MF, Heneine LG, Mansur HS. Biocompatibility evaluation of hydroxyapatite/collagen nanocomposites doped with Zn^{+2}. Biomed Mater 2007;2:135-141.

Received May 8, 2016
Accepted October 17,2016